Effects of Loading Rate and Thickness on Mixed-Mode I/II Fracture Toughness of Thermoset Epoxy Resin

C. Kanchanomai, S. Rattananon

Department of Mechanical Engineering, Faculty of Engineering, Thammasat University, Pathumthani 12120, Thailand

Received 18 April 2007; accepted 18 February 2008
DOI 10.1002/app.28330
Published online 7 May 2008 in Wiley InterScience (www.interscience.wiley.com).

ABSTRACT: The influences of loading rate and thickness on fracture behavior and mechanism of thermoset epoxy resin with polyamine hardener under mixed-mode (mode I/II) loading have been studied at low thickness and low loading rate (LTLL), as well as high thickness and high loading rate (HTHL). Under the variation of mixed-mode loading from mode I to mode II, fracture toughness of HTHL specimens were under plane-strain condition. For LTLL specimens, the fracture toughness at dominated mode I loading was under plane-stress condition, whereas those at dominated mode II loading were under plane-strain condition. The stretched zone due to the principal stress in the normal direction to the crack plane as well as shear lips due to the Poisson contraction in the thickness direction were the main characteristic of the fracture surface of LTLL specimen tested at pure mode I loading. On the other hand, the mirror-like fracture surface was observed for the HTHL specimen tested at pure mode I loading. Under pure mode II loading, the aligned stretched zone due to the maximum shear stress was the main characteristic of the fracture surface of LTLL specimen, whereas irregular appearance of the stretched zone was observed for the HTHL specimen. © 2008 Wiley Periodicals, Inc. J Appl Polym Sci 109: 2408–2416, 2008

Key words: fracture; mechanical properties; thermosets; toughness

INTRODUCTION

Epoxy resins generally have low shrinkage after curing, low moisture absorption, and wide range of operating temperature (−25 to 150°C). Moreover, the large number of compounds can react with the epoxy ring to form resin systems with a very wide range of properties,[1–3] therefore it has been used as a matrix in various polymer-matrix composites. During services, the engineering polymers fail to perform their structural function if they have excessive deformation or fracture. Without any significant discontinuities within a part, the deformation distributes uniformly on the load bearing area, and the part is likely to fail by excessive deformation. On the other hand, localized plastic deformation could occur around the discontinuities of a part. If the critical condition is reached, the part is likely to fail by fracture. These discontinuities could be the defects during production, cracks during service, or complex geometry of product.

Based on the concept of fracture mechanics, every linear elastic material has a fracture toughness called the critical stress intensity factor (K_c). Fracture of a part will occur if the stress intensity factor (K) equals or exceeds the K_c of the material. The K is a fracture mechanics parameter around crack tip, i.e., a function of crack size, geometry, and applied load. While the K_c is a property of material and depends on various variables, e.g., loading rate, geometry, loading mode, temperature, environment, and stress system. During service, there are three types of loading mode that a crack can experience. Mode I loading is the principal load that applied normal to the crack plane, and can open the crack. Mode II loading is an in-plane shear loading that can slide one crack surface with respect to the other. Lastly, mode III loading is an out-of-plane shear loading that can tear one crack surface with respect to the other. The fracture toughness varies with the loading mode, i.e., K_{IIc} and K_{IIIc} are generally greater than K_{Ic}.[4] The fracture toughness also depends on the stress system. Under mode I loading, the plane-strain dominated condition around crack tip could occur for a thick part, which results in poor fracture resistance or low fracture toughness. While the plane-stress dominated condition around crack tip could occur for a thin part, which results in high fracture toughness.[5]

The fracture toughness of modified diglycidyl ethers bisphenol-A resin with the modified aliphatic

Correspondence to: C. Kanchanomai (kchao@engr.tu.ac.th).
Contract grant sponsor: Thailand Research Fund, National Research Council of Thailand, and Commission on Higher Education of Thailand.

amine hardener have been previously studied at loading rates of 10^{-1}–10^{3} mm/min.[6] The critical stress intensity factor and critical strain energy release rate were high and stable at low loading rates (plane-stress fracture toughness), and became low and stable at high loading rates (plane-strain fracture toughness) with the transition of loading rate at $\sim$ 10 mm/min. Low and Mai[7] studied the failure mechanisms of several epoxy polymers (including pure, rubber, and particulate modified, as well as rubber/particulate hybrid epoxies) over a wide range of strain rates (10^{-6}–10^{2} sec^{-1}) and temperatures (-80 to 60°C). They found that the plastic-induced crack blunting mechanisms resulted in the variation of critical strain energy release rate with strain rate. The fracture behavior of an isotactic polypropylene has been investigated at test speeds between 0.1 mm/s and 14 m/s by Gensler et al.[8] The iPP homopolymer displayed a ductile-brittle transition with increasing test speed. Highly dissipative shear processes dominated at low speeds, multiple crazing dominated at intermediate speeds, whereas crack tip damage was limited to a single localized deformation zone (single crack-tip craze) at high speeds. Morgan and O'Neal[9] studied the relationship between the structure, microscopic flow, and failure processes of diethylene triamine-cured bisphenal-A-diglycidyl ether epoxies. The epoxy films deformed and failed by a crazing process, i.e., coarse fracture topography with coarse fibrils for poorly developed crazes, and mirror-like fracture topography with fine fibrils for well-developed crazes. D'Almeida and Monteiro[10] analyzed the topographic marks left at the fracture surfaces of epoxy resins with various resin/hardener ratios. The amine-rich (hardener-rich) compositions showed an unexpected deformation capacity, and the development of a tear zone and striations were found on their fracture surface. On the other hand, featureless fracture surfaces were observed for the epoxy-rich compositions. Araki et al.[11] investigated the fracture under mixed mode I/II for epoxy resin at room temperature and 3 μm/s displacement rate. They found that the relaxation effect on fracture toughness varies with the mode mixity, and so the common fracture criteria for mixed mode could not be applied to the epoxy resin. In contrast, the crack initiation angle can possibly be determined independently of the relaxation effect.

For particle-filled epoxies and fiber-filled epoxies, it is known that the fracture mechanisms depend on reinforcement (size, morphology, volume fraction), interfacial bonding, phase transformation, and mechanical properties (matrix and reinforcement).[12–15] Unfortunately, limited amount of works have been done on the fracture behavior and mechanism of pure epoxy resin. The influences of loading rate and thickness on fracture behavior and mechanism of thermoset epoxy resin with polyamine hardener under mixed-mode (mode I/II) loading were therefore investigated in this work. The fracture toughness (K_{IQ} and K_{IIQ}) were obtained from the mixed-mode (mode I/II) fracture toughness tests at low thickness and low loading rate condition (high deformation), as well as high thickness and high loading rate condition (low deformation). The results were correlated with the analysis of fracture surfaces, and then the fracture behavior and mechanism were discussed.

MATERIAL AND EXPERIMENTAL PROCEDURE

Thermoset epoxy resin with polyamine hardener (Thai Epoxy and Allied Products Company, Thailand) was used in this work. The DGEBA (diglycidyl ethers bisphenol-A) resin and the aliphatic amine hardener were initially mixed (100 : 35 resin/hardener weight ratio), and then cured at ambient temperature for 24 h to the form of flat sheets (4- and 7-mm thickness). The postcuring was performed in air circulating oven at 80°C for 4 h to achieve the optimum mechanical strength. The geometry of specimen and preparation of notch were in accordance with the ISO 13586: Plastic—Determination of fracture toughness (G_{IC} or K_{IC}).[16] The specimens, i.e., single edge-notch bending (SENB) specimens, were machined from a sheet to the dimension shown in Figure 1. The original crack (a_o) was introduced by saw machine to obtain a notch, and then a fresh razor blade was slid over the tip of the notch to obtain $\sim$ 0.1-mm initial crack tip radius.

For pure mode I loading, the fracture toughness tests were performed following the ISO 13586 standard.[16] Unfortunately, there was no standard practice written for the fracture toughness test under mixed-mode (mode I/II) loading. However, there were a number of works that analytically and numerically studied the mixed-mode (mode I/II) fracture toughness, and confirmed the results by experiments using various materials. In this work, the fracture toughness tests under mixed-mode (mode I/II) loading have been performed following the procedures proposed by Fett,[17] Choi et al.,[18] He and Hutchinson,[19] and Murakami.[20] These procedures included the experimental configuration, empirical formulas for stress state at the crack tip, and geometry functions for stress intensity factor.

Under mode I loading, the fracture toughness of epoxy resin was high and stable at low loading rates (plane-stress fracture toughness), and became low and stable at high loading rates (plane-strain fracture toughness) with the transition of loading rate at

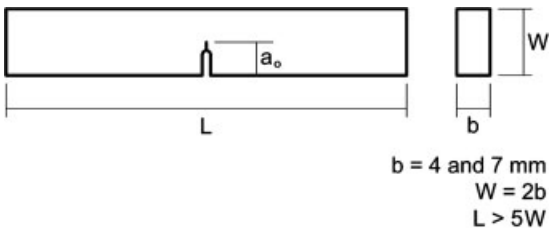

Figure 1 Geometry of a single edge-notch bending (SENB) specimen.

$\sim$ 10 mm/min.[6] Therefore, the effects of loading rate and thickness on mixed-mode (mode I/II) fracture toughness were studied using the specimens with 4-mm thickness and 10^{-1} mm/min loading rate (low thickness and low loading rate, LTLL), as well as specimens with 7-mm thickness and 10^{3} mm/min loading rate (high thickness and high loading rate, HTHL), respectively. All fracture toughness tests were performed on a servo-hydraulic fatigue machine at 55% relative humidity, and a constant temperature of 25°C. The load, displacement, and time were simultaneously recorded with a personal computer-controlled data acquisition system during the tests. To reduce the effect of variation of cross-link density on the fracture toughness,[9] the fracture toughness tests in each condition have been repeated five times, and the average K_{IQ} and K_{IIQ} were determined. After failure, the fracture surfaces were examined under both optical microscope and scanning microscope.

CALCULATION OF FRACTURE TOUGHNESS

The condition of mixed-mode (mode I/II) loading at the tip of original crack can be defined using the angle of mode mixity (β) as follows:

$$\beta = \tan^{-1}\left(\frac{K_{IIQ}}{K_{IQ}}\right) \tag{1}$$

where K_{IQ} is the fracture toughness under opening mode (mode I) loading, and K_{IIQ} is the fracture toughness under shearing mode (mode II) loading. The β is 0° for pure mode I loading and becomes 90° for pure mode II loading. To obtain the mixed-mode fracture toughness, three types of bending fracture toughness tests (Fig. 2) were preformed, as follows.

Three-point bending test of asymmetric precracked specimen (3PBTA)

The mixed-mode stress intensity factor around the tip of original crack can be manipulated by adjusting the distance (s) from the line of applied load (P) to the original crack, as shown in Figure 2(a). The K_{IQ} and K_{IIQ} can be determined as follows:[17]

$$K_{IQ} = \sigma_c F_I \sqrt{\pi a_o} \tag{2}$$

$$K_{IIQ} = \sigma_c F_{II} \sqrt{\pi a_o} \tag{3}$$

$$\sigma_c = \frac{3P_c A}{W^2 b} \tag{4}$$

$$F_I = F_I' \cdot (1 - a_o/W)^{-3/2} \tag{5}$$

$$F_{II} = F_{II}' \cdot (1 - a_o/W)^{-1/2} \tag{6}$$

where F_I' and F_{II}' are the geometric functions, P_c is the maximum applied load, and σ_c is the maximum applied stress calculated using the beam theory. Based on an analytical solution for stress state

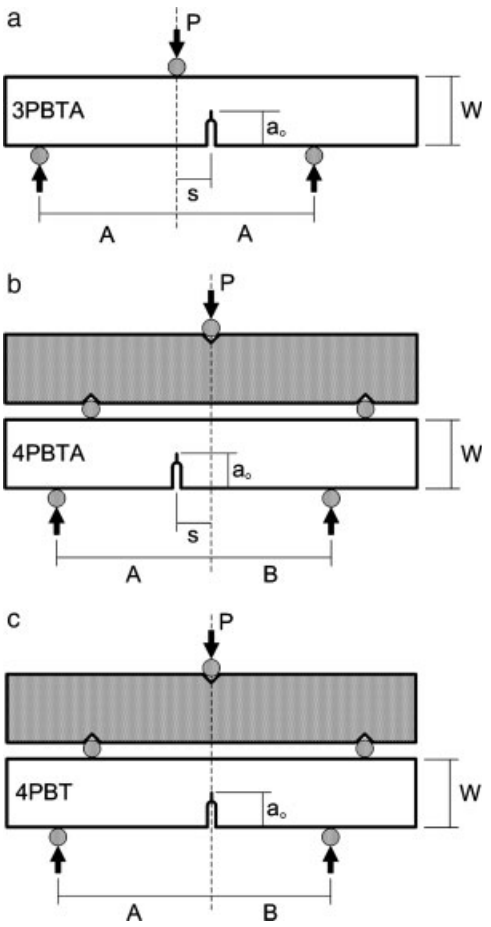

Figure 2 (a) 3-point bending test of asymmetric precracked (3PBTA) specimen, (b) 4-point bending test of asymmetric precracked (4PBTA) specimen, and (c) 4-point bending test of symmetric precracked (4PBT) specimen.

TABLE I
The Loading Configuration of Mixed-Mode I/II Fracture Toughness Tests

	LTLL (4 mm thickness and 0.1 mm/min)					HTHL (7 mm thickness and 1000 mm/min)				
Fracture toughness test	a_o/W	s (mm)	A (mm)	B (mm)	β^o	a_o/W	s (mm)	A (mm)	B (mm)	β^o
3PBTA	0.50	0	16	–	0.0	0.50	0	28	–	0.0
	0.60	10	16	–	10.5	0.50	16	28	–	9.7
	0.60	13	16	–	23.7	0.50	22	28	–	18.0
	0.60	14	16	–	29.5	0.50	24	28	–	35.7
	0.40	14	16	–	37.2					
4PBTA	0.30	3	16	8	21.4	0.60	5	14	7	25.6
	0.30	2	16	8	30.3	0.60	3	14	7	41.6
	0.70	1	16	8	41.5	0.20	2	14	7	47.7
	0.50	1	16	8	50.7					
4PBT	0.15	–	20	4	61.5	0.15	–	35	7	61.7
	0.20	–	20	4	71.1	0.20	–	35	7	70.3
	0.30	–	20	4	81.5	0.30	–	35	7	81.2
	0.80	–	20	4	89.8	0.80	–	35	7	89.8

around crack tip, the geometric functions (F_I' and F_{II}') for various a_o/W and s/A were calculated and given by Fett.[17] The loading configuration of the 3PBTA tests as well as the obtained angle of mode mixity (β) are summarized in Table I. The crack was subjected to pure mode I loading for $s = 0$, i.e., the loading configuration of 3PBTA test was similar to that recommended by the ISO 13586 standard.[16]

Four-point bending test of asymmetric precracked specimen (4PBTA)

The mixed-mode stress intensity factor around the tip of original crack can be manipulated by adjusting the distance (s) from the line of applied load (P) to the original crack, as shown in Figure 2(b). The K_{IQ} and K_{IIQ} can be determined as follows:[18]

$$K_{IQ} = \sigma_c F_I \sqrt{\pi a_o} \tag{7}$$

$$K_{IIQ} = \tau_c F_{II} \sqrt{\pi a_o} \tag{8}$$

where F_I and F_{II} are the geometric functions, σ_c is the maximum applied normal stress, and τ_c is the maximum applied shear stress. Based on an analytical solution for stress state around crack tip, the F_I and F_{II} for various a_o/W were calculated and given by He and Hutchinson.[19] While the σ_c and τ_c can be determined from the beam theory as follows:

$$\sigma_c = \frac{A-B}{A+B} \cdot \frac{6sP_c}{W^2 b} \tag{9}$$

$$\tau_c = \frac{A-B}{A+B} \cdot \frac{P_c}{Wb} \tag{10}$$

where P_c is the maximum applied load. The loading configuration of the 4PBTA tests as well as the obtained angle of mode mixity (β) are summarized in Table I.

Four-point bending test of symmetric precracked specimen (4PBT)

The mixed-mode stress intensity factor around the tip of original crack can be manipulated by using

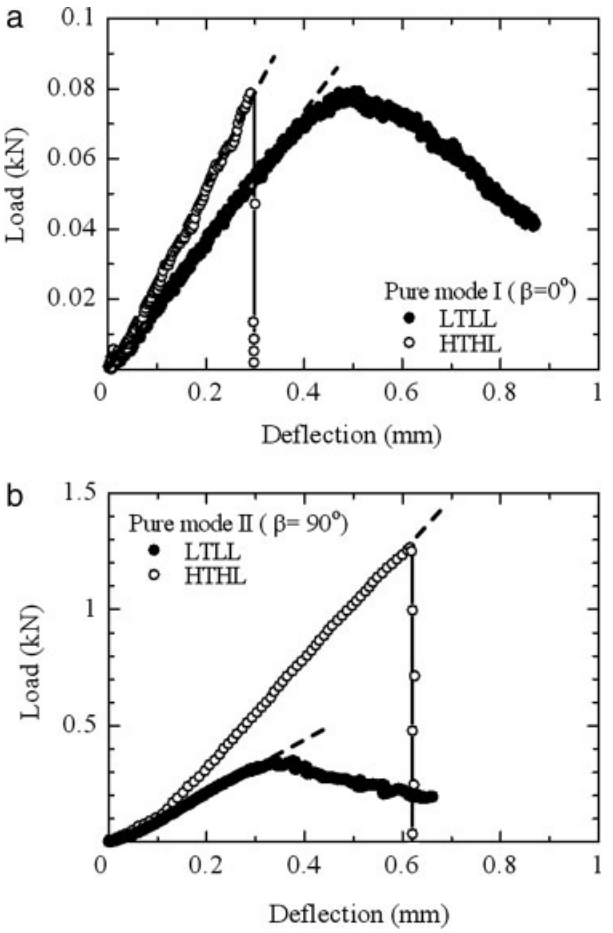

Figure 3 Relationships between applied load and deflection in the direction of applied load of; (a) LTLL and HTHL specimens tested under pure mode I loading, and (b) LTLL and HTHL specimens tested under pure mode II loading.

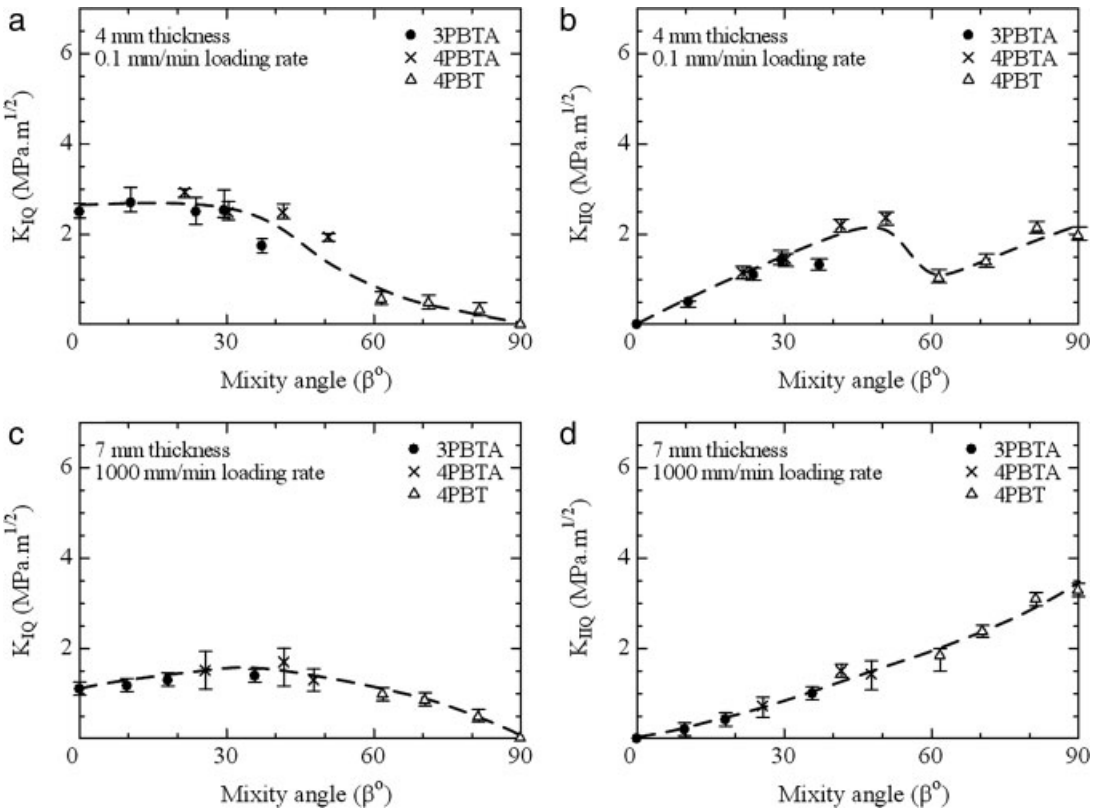

Figure 4 (a) Relationship between mode I fracture toughness (K_{IQ}) and mixity angle of LTLL specimens, (b) Relationship between mode II fracture toughness (K_{IIQ}) and mixity angle of LTLL specimens, (c) Relationship between mode I fracture toughness (K_{IQ}) and mixity angle of HTHL specimens, and (d) Relationship between mode II fracture toughness (K_{IIQ}) and mixity angle of HTHL specimens.

specimens with various original crack sizes (a_o), as shown in Figure 2(c). The K_{IQ} and K_{IIQ} can be determined as follows:[20]

$$K_{IQ} = \tau_c F_I \sqrt{\pi a_o} \tag{11}$$

$$K_{IIQ} = \tau_c F_{II} \sqrt{\pi a_o} \tag{12}$$

where F_I and F_{II} are the geometric functions, and τ_c is the maximum applied shear stress. Based on an analytical solution for stress state around crack tip, the F_I and F_{II} for various a_o/W were given in the stress intensity factors handbook.[20] While the τ_c can be determined from the beam theory as follows:

$$\tau_c = \frac{P_c}{Wb} \cdot \left(\frac{1 - B/A}{1 + B/A}\right) \tag{13}$$

where P_c is the maximum applied load. For $a_o/W = 0.8$, the original crack was subjected to pure mode II loading. The loading configuration of the 4PBT tests as well as the obtained angle of mode mixity (β) are summarized in Table I.

RESULTS AND DISCUSSION

Load-deflection relationship

Relationships between applied load and deflection of LTLL and HTHL epoxy resins under pure mode I loading and pure mode II loading are shown in Figure 3(a,b), respectively. The load and deflection plots could be divided into three stages, i.e., linearly increased stage (elastic deformation), nonlinearly increased stage (plastic deformation), and a drop when load reached the maximum level (starting of crack propagation). The evidence of plastic deformation could be clearly seen for LTLL specimens, whereas a sudden drop after linearly increased stage was observed for HTHL specimens. These observations corresponded to the fact that the deformation mechanism of amorphous polymer, e.g., epoxy resin, is time-dependent. With increasing loading rate, the time for time-dependent deformation process decreased, and became dominated time-independent deformation process after the loading rate reached 10^2 mm/min.[6] For both LTLL and HTHL specimens, the maximum applied loads (P_c) under pure mode II loading were higher than those of pure mode I loading. It is confirmed that

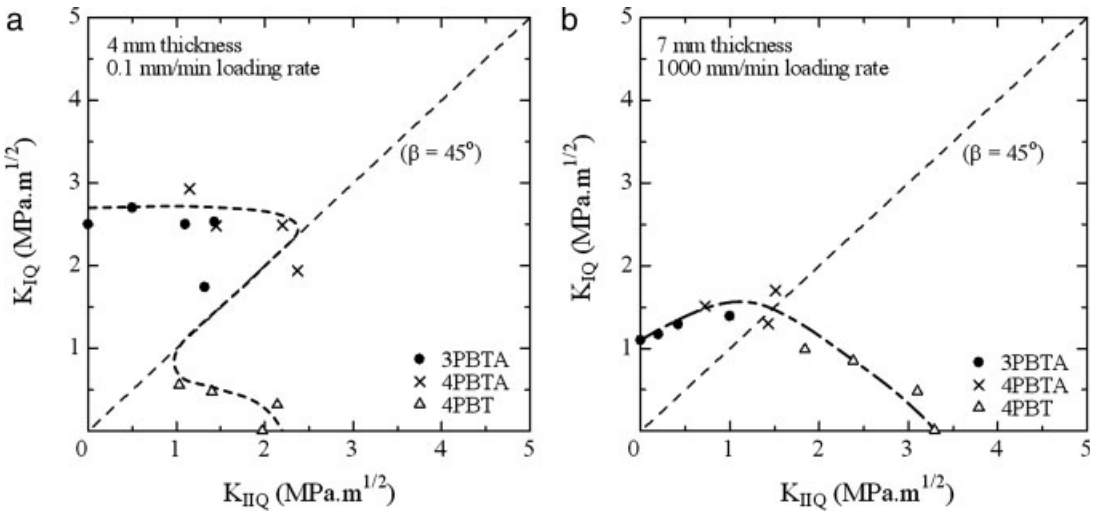

Figure 5 Relationships between fracture toughness under mode I loading (K_{IQ}) and fracture toughness under mode II loading (K_{IIQ}) of; (a) LTLL specimens, and (b) HTHL specimens.

the stress–strain field at the crack tip under mode I loading was more severe than that under mode II loading.

Fracture toughness

Relationships between fracture toughness (K_{IQ} and K_{IIQ}) and mode-mixity angle (β) of both LTLL and HTHL specimens are shown in Figure 4(a–d). The K_{IQ} was high at pure mode I loading (β = 0), decreased with increasing mode-mixity angle, and became zero at pure mode II loading (β = 90°), as shown in Figure 4(a,c). On the other hand, the K_{IIQ} showed opposite behavior, i.e., zero at pure mode I loading (β = 0°) and increased with increasing mode-mixity angle [Fig. 4(b,d)]. However, a drop of K_{IIQ} during 50° < β < 60° was observed for LTLL specimens [Fig. 4(b)].

The relationships between K_{IQ} and K_{IIQ} of LTLL and HTHL specimens are shown in Figure 5(a,b), respectively. The 45° dash lines, above which are the regimes of dominated mode I loading and below which are the regimes of dominated mode II loading, are added into Figure 5(a,b). Under the regime of dominated mode I loading, the K_{IQ} of LTLL specimens was insensitive to the increasing of K_{IIQ}, whereas marginal increasing of K_{IQ} of HTHL specimens with increasing K_{IIQ} was observed. Under the regime of dominated mode II loading, the influence of K_{IQ} on the K_{IIQ} was clear for both LTLL and HTHL specimens. During the transition from the regime of dominated mode I loading to the regime of dominated mode II loading (β = 45°), the abrupt change in relationship between K_{IQ} and K_{IIQ} was observed for LTLL specimens [Fig. 5(a)]. For comparison, the relationship between K_{IQ} and K_{IIQ} of LTLL and HTHL specimens are shown together in Figure 6. Under the regime of dominated mode I loading, the fracture toughness of HTHL specimens were lower than that of LTLL specimens. The opposite behavior was observed for epoxy resins under the regime of dominated mode II loading, i.e., the fracture toughness of HTHL specimens were higher than that of LTLL specimens.

For a sharp crack, it is known that the stress–strain field at crack tip under opening mode loading (mode I) is more severe than that under shearing mode loading (mode II). The fracture resistance of material under dominated mode I loading is therefore lower than that under dominated mode II loading, i.e., the K_{IQ} is lower than K_{IIQ}.[4] This behavior

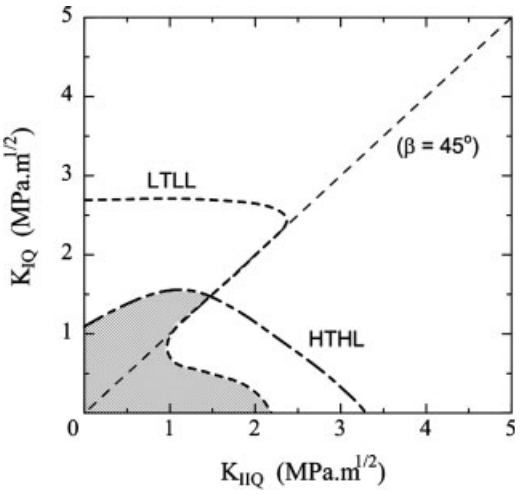

Figure 6 Relationships between fracture toughness under mode I loading (K_{IQ}) and fracture toughness under mode II loading (K_{IIQ}).

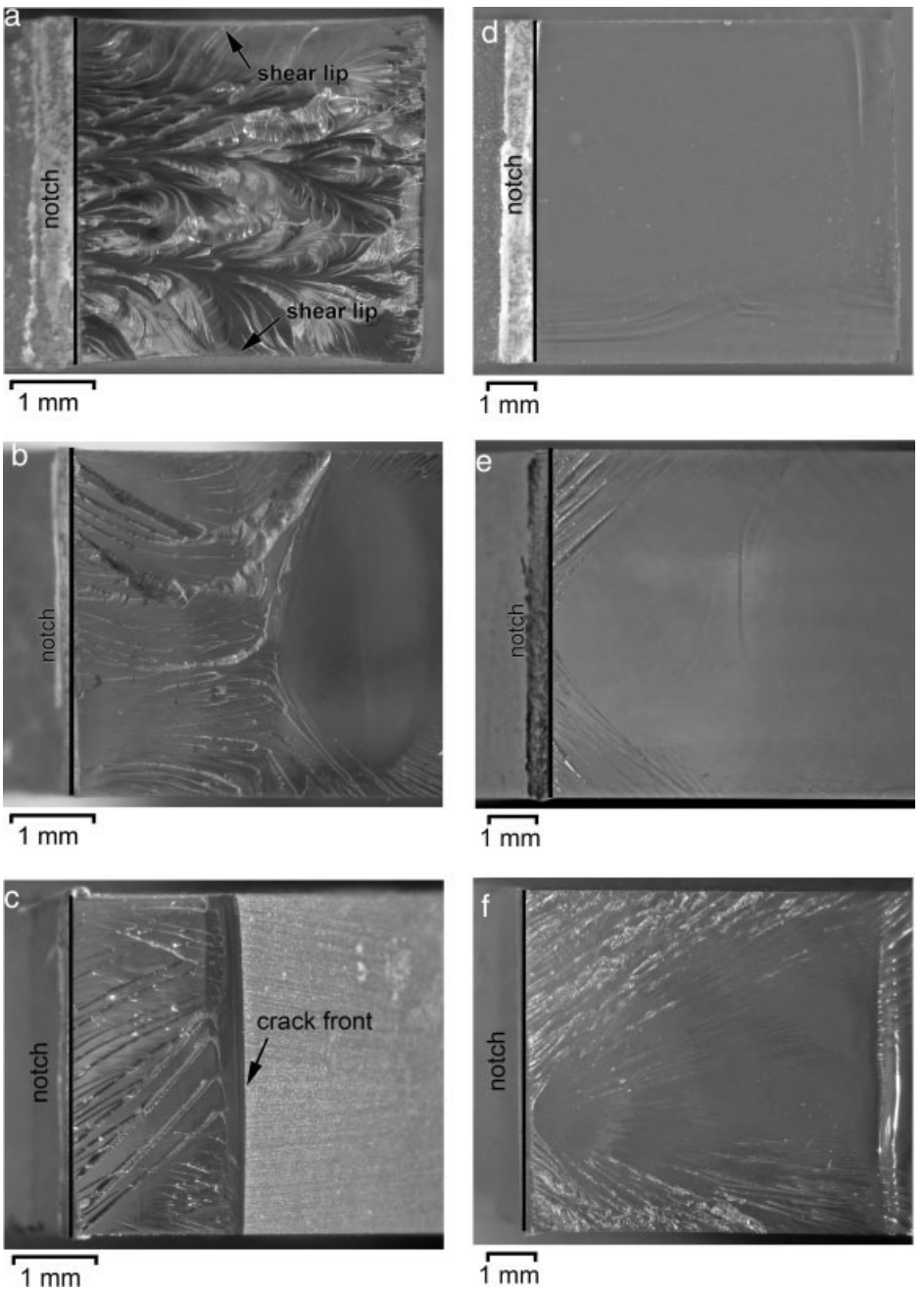

Figure 7 Micrographs of fracture surfaces of (a) LTLL specimen tested under pure mode I loading, (b) LTLL specimen tested under mixed-mode loading ($\beta = 40^\circ$), (c) LTLL specimen tested under pure mode II loading, (d) HTHL specimen tested under pure mode I loading, (e) HTHL specimen tested under mixed-mode loading ($\beta = 30^\circ$) and (f) HTHL specimen tested under pure mode II loading (cracks propagated from left to right).

corresponded to the present fracture toughness obtained from the HTHL specimens, as shown in Figure 5(b). However, opposite behavior was observed for LTLL specimens. At dominated mode I loading, the Poisson contraction in the thickness direction was likely to occur around the crack tip of the LTLL specimens because of the lack of constraint on the time-dependent deformation. The state of strain around the crack tip was three-dimensional, whereas the state of stress around the crack tip was two-dimensional (plane stress). Significant plastic deformation in the vicinity of crack tip resulted in the increasing of crack tip radius (crack blunting), the stress around the crack tip decreased, and the fracture resistance was improved. The fracture toughness of LTLL specimens under dominated mode I loading were therefore higher than those of dominated mode II loading [Fig. 5(a)]. For HTHL speci-

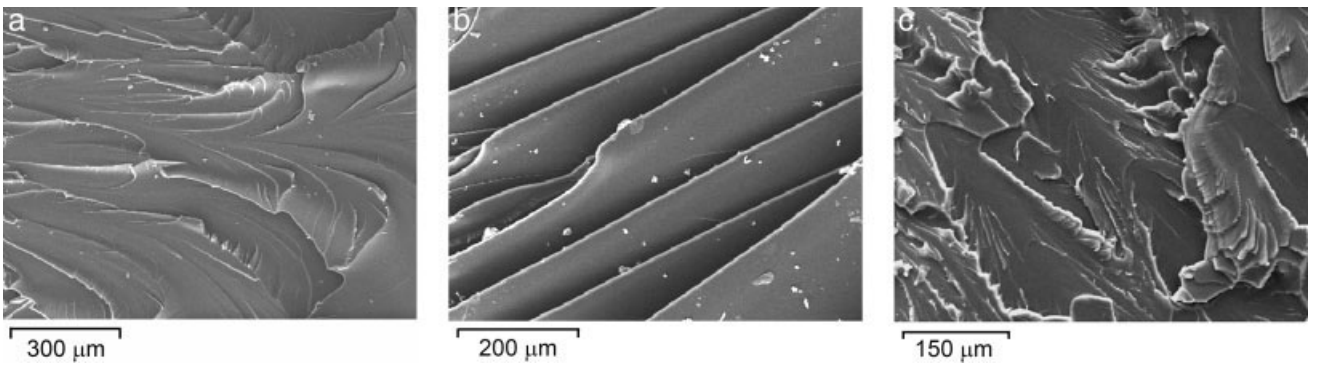

Figure 8 Micrographs of fracture surfaces (a) the stretched zone due to the principal stress of LTLL specimen tested under pure mode I loading, (b) the aligned stretched zone due to the maximum shear stress of LTLL specimen tested under pure mode II loading, and (c) the irregular appearance of stretched zone due to the maximum shear of HTHL specimen tested under pure mode II loading (cracks propagated from left to right).

mens under dominated mode I loading, the plane stress condition in the vicinity of crack tip could not occur, and their fracture toughness became lower than those of the LTLL specimens (Fig. 5(b)).

Unlike the crack tip under mode I loading, the fractures of both LTLL and HTHL specimens tested at dominated mode II loading were not controlled by crack blunting because the Poisson contraction could not occur under shear loading. The fracture process then depended on the two-dimensional deformation in the vicinity of crack tip. As there was more time for the localized plastic deformation processes around the crack tip, the deformation for LTLL specimen tested at dominated mode II loading was higher than that of HTHL specimen. Thus, the K_{IIQ} of LTLL specimens tested at dominated mode II loading were lower than those of HTHL specimens (Fig. 6).

Since the fracture mechanism of LTLL specimens changed from the Poisson contraction—controlled mechanism under the regime of dominated mode I loading to the shear strain—controlled mechanism under the regime of dominated mode II loading, the abrupt change in relationship between K_{IQ} and K_{IIQ} at $\beta = 45^\circ$ was observed in Figure 5(a). A safe area (below which the fracture could not occur) was indicated by shadow area in Figure 6. Under the dominated mode I loading, the fracture toughness of HTHL specimens could be used as the fracture criteria, whereas the fracture toughness of LTLL specimens could be used as the fracture criteria under the dominated mode II loading.

Fracture surface

Micrographs of fracture surfaces of LTLL and HTHL specimens tested at pure mode I loading, mixed-mode (mode I/II) loading, and pure mode II loading are shown in Figure 7(a–f). The Poisson contraction in the thickness direction (shear lips) could be observed on the side surfaces of LTLL specimens tested at pure mode I loading [Fig. 7(a)], whereas no shear lip could be seen for the others. As an evidence of ductile fracture, the stretched zone due to the principal stress in the normal direction to the crack plane was also observed on the fracture surface of LTLL specimens tested at pure mode I loading [Fig. 7(a)]. The detail of the stretched zone due to the principal stress is shown in Figure 8(a). Together with the plastic deformation observed in the load-deflection curve [Fig. 3(a)] and the high value of K_{IQ} (Fig. 6), it is confirmed that the fracture process of the LTLL specimen tested at pure mode I loading was dominated by the plane-stress condition (ductile fracture). With the increasing of mode-mixity angle, the area of the stretched zone due to the principal stress decreased, and became the stretched zone due to the maximum shear stress in the tangential direction to the crack plane for the LTLL specimen tested at pure mode II loading [Fig. 7(c)]. The detail of the stretched zone due to the maximum shear stress is shown in Figure 8(b).

Unlike the LTLL specimens, the mirror-like fracture surface was observed for the HTHL specimen tested at pure mode I loading [Fig. 7(d)]. Together with the sudden fracture observed in the load-deflection curve [Fig. 3(a)], the fracture process of the HTHL specimen tested at pure mode I loading was therefore dominated by the plane-strain condition (brittle fracture), i.e., low K_{IQ} (Fig. 6). With the increasing mode-mixity angle, the mirror-like fracture surface decreased, and became a combination between mirror-like surface and stretched zone due to the maximum shear stress for the HTHL specimen tested at pure mode II loading [Fig. 7(f)]. As there was less time for the deformation of HTHL specimen tested at pure mode II loading, the stretched zone due to the maximum shear stress simultane-

ously occurred on the fracture surface, and showed an irregular appearance [Fig. 8(c)] comparing to more aligned stretched zone of LTLL specimen [Fig. 8(b)].

CONCLUSIONS

The influences of loading rate and thickness on fracture behavior and mechanism of thermoset epoxy resin with polyamine hardener under mixed-mode (mode I/II) loading have been studied at low thickness and low loading rate (LTLL), as well as high thickness and high loading rate (HTHL). The main conclusions are summarized as follows:

1. The fracture toughness of HTHL specimens at all mode-mixity angles ($0^\circ \leq \beta \leq 90^\circ$) were under plane-strain condition, and the fracture toughness at dominated mode I loading were lower than those at dominated mode II loading. On the other hand, the fracture toughness of LTLL specimens tested at dominated mode I loading was under plane-stress condition, whereas those tested at dominated mode II loading were under plane-strain condition. The fracture toughness of LTLL specimens at dominated mode I loading was higher than those at dominated mode II loading. Under the dominated mode I loading, the fracture toughness of HTHL specimens could be used as the fracture criteria, whereas the fracture toughness of LTLL specimens could be used as the fracture criteria under the dominated mode II loading.
2. The fracture surface of LTLL specimens tested at pure mode I loading (plane-stress fracture) showed the stretched zone due to the principal stress in the normal direction to the crack plane as well as shear lips due to the Poisson contraction in the thickness direction. On the other hand, the mirror-like fracture surface was observed for the HTHL specimen tested at pure mode I loading (plane-strain fracture). Unlike the fracture surfaces of specimens tested at pure mode I loading, the stretched zone due to the maximum shear stress simultaneously occurred on the fracture surface, and showed an irregular appearance for the HTHL specimen tested at pure mode II loading. While more aligned stretched zone was observed for the LTLL specimen tested at pure mode II loading.

The authors acknowledge the discussions and supports from Professor Y. Mutoh (Nagaoka University of Technology), and Dr. M Soni (Thai Epoxy and Allied Products Company, TEC).

References

1. Crawford, R. J. Plastics Engineering; Butterworth-Heinemann: Oxford, 1998.
2. Margolis, J. M. Advanced Thermoset Composites—Industrial and Commercial Applications; Van Nostrand Reinhold: New York, 1985.
3. Mills, N. J. Plastics: Microstructure and Engineering; Arnold: London, 1993.
4. Anderson, T. L.; Fracture Mechanics: Fundamental and Applications; CRC Press: New York, 1994.
5. Dowling, N. E. Mechanical Behavior of Material: Engineering Methods for Deformation, Fracture, and Fatigue; Prentice-Hall International: New Jersey, 1993.
6. Kanchanomai, C.; Rattananon, S.; Soni, M. Polym Test 2005, 24, 886.
7. Low, I. M.; Mai, Y. W. J Mater Sci 1989, 24, 1634.
8. Gensler, R.; Plummer, C. J. G.; Grein, C; Kausch, H. H. Polymer 2000, 41, 3809.
9. Morgan, R. J.; O'Neal, J. E. J Mater Sci 1966, 12, 1977.
10. D'Almeida, J. R. M.; Monteiro, S. N. J Mater Sci Lett 1996, 15, 955.
11. Araki, W.; Nemoto, K.; Adachi, T.; Yamaji, A. Acta Mater 2005, 53, 869.
12. Matthews, F. L.; Rawlings, R. D. Composite Materials: Engineering and Science; Chapman & Hall: London, 1994.
13. Araki, W.; Adachi, T.; Yamaji, A. Mater Sci Forum 1985 2003, 426.
14. Lee, D. B.; Ikeda, T.; Miyazaki, N.; Choi, N. S. Eng Fract Mech 2002, 69, 1363.
15. Kim, H. S.; Khamis, M. A. Compos A 2001, 32, 1311.
16. ISO 13586. Plastics—Determination of fracture toughness (G_{IC} and K_{IC})—Linear elastic fracture mechanics (LEFM) approach; International Organization for Standardization: Switzerland; 2000.
17. Fett, T. Int J Fract 1991, 48, R67.
18. Choi, S. R.; Zhu, D.; Miller, R. A. Eng Fract Mech 2005, 72, 2144.
19. He, M. Y.; Hutchinson, J. W. J Appl Mech 2000, 67, 207.
20. Murakami, I. Stress Intensity Factors Handbook; Pergamon Press: New York, 1987.